

Electronic Supplementary Information (ESI)

Metal-Free Graphitic Carbon Nitride/Carbon-Dots Composites: Unveiling Mechanochemical Synthesis Opportunities

Ilaria Bertuol,¹⁺ Lucía Jiménez-Rodríguez,²⁺ Rafael R. Solís,² Patrizia Canton,¹ Maurizio Selva,¹ Mónica Calero,² Alvise Perosa,¹ Daily Rodríguez-Padrón,^{1} Mario J. Muñoz-Batista,^{2*}*

¹ Dipartimento di Scienze Molecolari e Nanosistemi, Università Ca' Foscari di Venezia, 30123 Venezia, Italy

² Department of Chemical Engineering, University of Granada, 18074 Granada, Spain

D. R-P. (daily.rodriguez@unive.it), M.J. M-B. (mariomunoz@ugr.es)

⁺ These authors have contributed equally to this work.

Abstract:

Environmentally friendly, metal-free photocatalysts offer a promising alternative to traditional metal-based semiconductors. In this study, we synthesised graphitic carbon nitride (CN) photocatalysts decorated with carbon dots (CDS) using two distinct methods: a hydrothermal approach and a solvent-free mechanochemical extrusion method. The resulting nanocomposites were thoroughly characterised for their physical, chemical, and optical properties and evaluated for photocatalytic activity in the selective oxidation of benzyl alcohol. Results revealed that the synthesis approach significantly impacted the composites' morphological and optical characteristics, affecting their photocatalytic performance. A light-matter interaction modelling study was further conducted to explore the relationship between optical properties and catalytic behaviour, offering valuable insights into the structure-function relationship of these novel photocatalysts. As a result, we present an alternative scheme to traditional synthesis and catalysis methods based on the use of high temperature and pressure conditions, which provides an energetically positive and environmentally friendly approach.

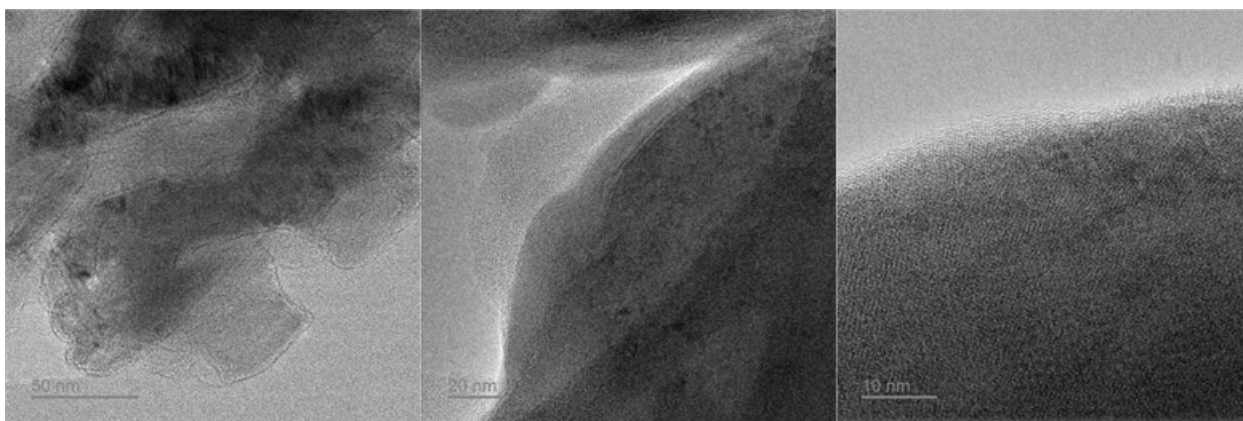


Figure S1. HR-TEM micrograph of the h-CN/g-CDS (nd) photocatalytic sample.

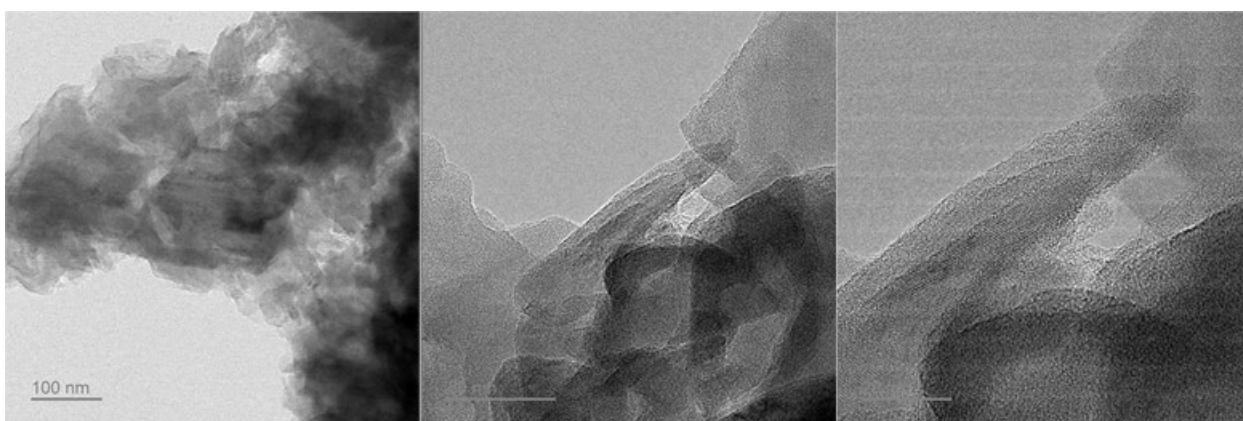


Figure S2. HR-TEM micrograph of the e-CN/a-CDS photocatalytic sample.

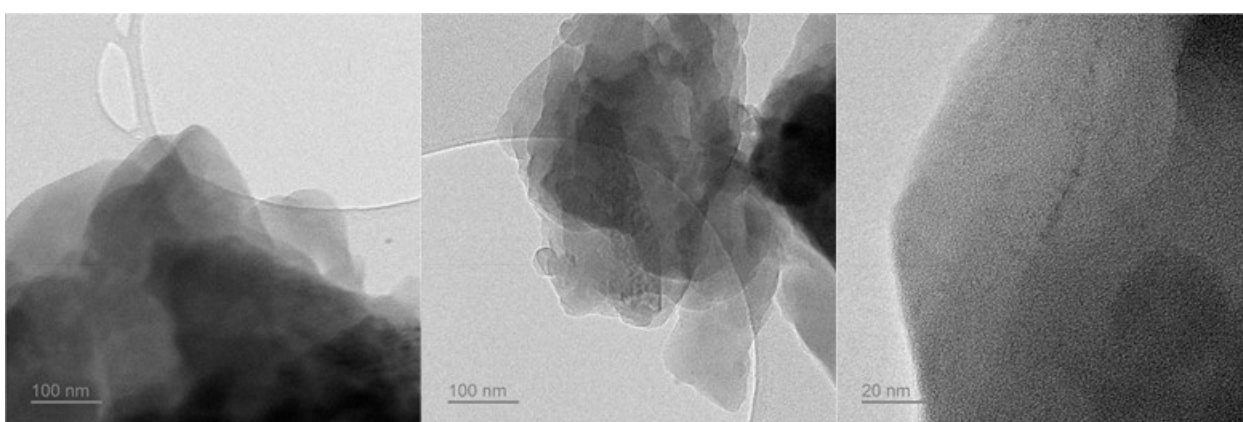


Figure S3. HR-TEM micrograph of the e-CN/g-CDS photocatalytic sample.

Table S1. Atomic %, C/N, O/N, and O/C ratio obtained by XPS.

Samples	C (at%)	N(at%)	O(at%)	C/N	O/N	O/C
CN	43.8	54.25	1.95	0.81	0.04	0.04
e-CN/a-CDS	48.78	44.93	6.29	1.09	0.14	0.13
e-CN/g-CDS (nd)	48.74	44.96	6.3	1.08	0.14	0.13
e-CN/g-CDS (d)	48.83	44.42	6.75	1.10	0.15	0.14
h-CN/a-CDS	48.54	47.08	4.38	1.03	0.09	0.09
h-CN/g-CDS (nd)	49.26	46.04	4.7	1.07	0.10	0.10
h-CN/g-CDS (d)	51.48	41.05	7.47	1.25	0.18	0.15

Light-matter interaction modelling

The average volumetric rate of photon absorption was obtained by solving the Radiative Transfer Equation (RTE) in the reactor system schematically presented in Figure 1 of the main text. The RTE measured the variation of intensity (associated to a beam of rays at wavelength λ in the direction of a solid angle vector $\underline{\Omega}$) through a direction of the space as described by Equation S1. The equation assumes; (i) the emission radiation is negligible (at room temperature), and (ii) steady state condition during the photocatalytic processes.

$$\frac{dI_{\lambda,\underline{\Omega}}(x)}{ds} = -\kappa_{\lambda}(x)I_{\lambda,\underline{\Omega}}(x) - \sigma_{\lambda}(x)I_{\lambda,\underline{\Omega}}(x) + \frac{\sigma_{\lambda}(x)}{4\pi} \int_{\Omega = 4\pi} p(\underline{\Omega}' \rightarrow \underline{\Omega}) I_{\lambda,\underline{\Omega}'} d\Omega \quad \text{S1}$$

To solve equation S1, it is necessary to determine, first, the optical properties of the photocatalysts suspensions. This is; (i) the spectral absorption coefficient (κ_{λ}), the spectral scattering coefficient (σ_{λ}), and the scattering phase function ($p(\underline{\Omega}' \rightarrow \underline{\Omega})$). To do it, the extinction coefficient of the samples ($\beta_{\lambda} = \sigma_{\lambda} + \kappa_{\lambda}$) was experimentally obtained by applying a standard linear regression to the plots of β_{λ} versus catalyst concentration C (6 concentrations from 0.25 – 1.5 g L⁻¹). To obtain the scattering phase function, and according with previous studies in similar catalysts (32), the Henyey and Greenstein phase function (Equation S2) was adopted.

$$p(\underline{\Omega}' \rightarrow \underline{\Omega}) = \frac{1 - g_{\lambda}^2}{(1 + g_{\lambda}^2 - 2g_{\lambda}^2 u_0)^{3/2}} \quad \text{S2}$$

In equation 3 g_{λ} is the so-called asymmetry factor and u_0 is the director cosine between incoming and outgoing light at each point of the space.

The optical properties were obtained by solving the RTE (which consider radiation absorption and scattering effect by the catalyst; Equation S1) using the discrete ordinate method (DOM) in rectangular 0.1-0.5 mm spectrophotometer cells in combination with a nonlinear, multiparameter regression procedure (lsqnonlin, Algorithm: Trust-Region-Reflective Optimization). Cells contain the liquid medium of the reaction, and such medium is subjected to agitation in exactly the same conditions used for measuring reaction rates. Considering that the cell can be represented as an infinite plane parallel medium with azimuthal symmetry, a one-dimensional, one-directional radiation transport model can be used to solve the RTE (see Figure S4A). This renders the g_λ , σ_λ and k_λ values as a function of the wavelength.

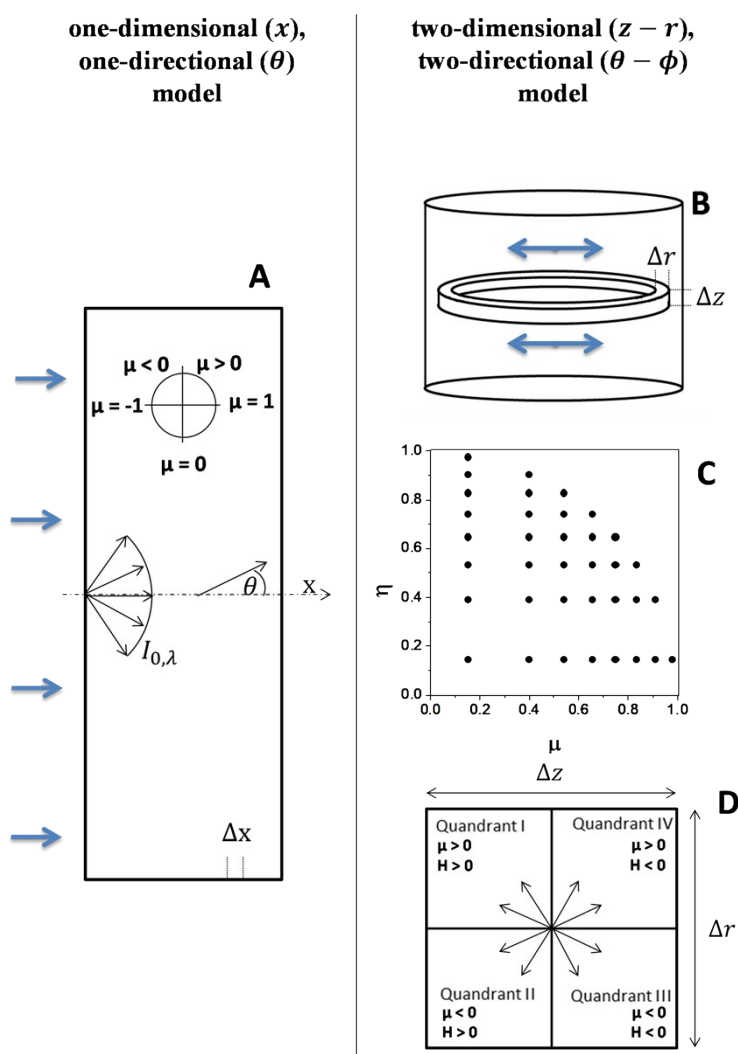


Figure S4. Schematic representation for the one-dimensional, one-directional radiation Model used for the spectrophotometer cell (A) and two-dimensional, two-directional radiation Model used for the

photoreactor (B-D). (B) Representation of the r and z spatial mesh discretization of the photoreactor, (C) Directional mesh for the Quadrant I and (D) representation of quadrants of directions as a function of the direction cosines (μ, η) respect to r and z axis in a cross section of the spatial cell.

Figure S4A thus shows a schematic representation of the spectrophotometer cell and the corresponding RTE solution scheme where the net light intensity is presented by one angular-related variable ($\mu = \cos(\theta)$) at each point of the cell one-dimensional (x variable) representation. The fitting procedure renders the values of ω_λ (the so-called albedo, defined in equation 4) and β_λ (equation S2) parameters that minimize the differences between model predictions and experimental data of diffuse transmittance and reflectance measurements at the spectrophotometric cell for a set of catalyst concentrations, C , and in the wavelength range of the light source. Then, the volumetric scattering and absorption coefficients can be obtained as following:

$$\sigma_\lambda = \beta_\lambda * \omega_\lambda \quad \text{S3}$$

$$\kappa_\lambda = \beta_\lambda - \omega_\lambda \quad \text{S4}$$

Once the optical properties of the catalyst(s) have been obtained, the evaluation of the radiation field inside the photoreactor can be carried out. The reactor is divided in three zones (defined by the position of the lamp ends) for the calculation. The three zones differ in the boundary conditions as well as the initial position at the radial (r) and axial (z) axis. The DOM tool was used to transform the integro-differential equation S1 into a system of algebraic equations that can be solved numerically until convergence (with a error below 1 % in each analyzed element of the observable) is reached. Our reactor configuration requires the use of a cylindrical two-dimensional ($z - r$ variables), two-directional ($\theta - \phi$ variables) model of the photoreactor radiation field (Figure S4B-C). The net radiation intensity at each $z - r$ point of the reactor is now represented using a discretized spatial mesh having two angular-related coordinates $\mu = \cos(\theta); \eta = \cos(\phi)$. Fig. SXC displays $\mu; \eta$ unitary, basal projection(s) in a quadrant of the space around a $z - r$ point calculated using the so-called S_{16} method. The determination of the intensity at each point of the reactor require to divide the space in 4 quadrants as depicted in Figure S4D and the measurement of the incident light intensity at the boundary (liquid surface) using actinometry. According to the Duderstadt and Martin recommendation and following the numerical

procedure scheme detailed by previous authors, the finite difference (DOM) was derived directly from the radiation balance at each mesh cell (Figure S5D).

Using the DOM approach the central intensity at each spatial cell (I_m^{ij}) can be calculated from the previous ones starting from the appropriate boundary values ($I_m^{i \pm 1/2, j}$; $I_m^{i, j \pm 1/2}$) as well as one “auxiliary” one coming from the so-called directional mesh ($I_{m-1/2}^{ij}$) as:

$$I_m^{ij} = |\mu_m|(A_{i,j+1/2} - A_{i,j-1/2})D^{-1}I_m^{i,j \pm 1/2} + 2|\eta_m|B_{i,j}D^{-1}I_m^{i \pm 1/2,j} + (A_{i,j+1/2} - A_{i,j-1/2}) \cdot (v_{m+1/2} + v_{m-1/2})W_m^{-1} + \kappa_\lambda V_{i,j} + \sigma_\lambda V_{i,j} D^{-1}W_m^{-1}I_{m-1/2}^{ij} + \frac{\sigma_\lambda}{4\pi} \sum_{n=1}^M I_n^{ij} P_{nm} W_n V_{i,j} D^{-1}$$

S5

Were

$$D = |\mu_m|(A_{i,j+1/2} - A_{i,j-1/2}) + 2|\eta_m|B_{i,j} + (A_{i,j+1/2} - A_{i,j-1/2}) \cdot (v_{m+1/2} + v_{m-1/2})W_m^{-1} + \kappa_\lambda V_{i,j} + \sigma_\lambda V_{i,j}$$

S6

$$A_{i+1/2,j} = 2\pi r_{i+1/2} \Delta z_j$$

S7

$$B_{i,j+1/2} = 2\pi \left(\frac{r_{i+1/2} + r_{i-1/2}}{2} \right) \Delta r_i$$

S8

$$V_{i,j} = 2\pi \left(\frac{r_{i+1/2} + r_{i-1/2}}{2} \right) \Delta z_j \Delta r_i$$

S9

The computational calculation at each quadrant of Figure XSD begins from the corner of the spatial mesh in which two of the four boundary conditions can be applied. In our case the four boundary conditions are: i) known inlet radiation for quadrants I and II at $z=0$; ii) null reflection in the inner reactor wall surfaces. The directional mesh at each spatial cell is always calculated in ascending m values, selecting as $m=1$ the angular direction more parallel to the r - z plane in which $I_{m-1/2}^{ij}$ is approximated to zero. With this extra condition and equation 11 the recursive equation 6 can be applied to the cell closer to the boundary conditions and so forth.

$$v_{m+1/2} - v_{m-1/2} = -\mu_m W_m$$

S10

For each quadrant, the complete set of 6 intensities required for each spatial mesh cell is obtained by applying equations 12-14.

$$I_m^{i,j} = \frac{(I_m^{i-1/2,j} + I_m^{i+1/2,j})}{2} \quad \text{S11}$$

$$I_m^{i,j} = \frac{(I_m^{i,j-1/2} + I_m^{i,j+1/2})}{2} \quad \text{S12}$$

$$I_m^{i,j} = \frac{(I_{m-1/2}^{i,j} + I_{m+1/2}^{i,j})}{2} \quad \text{S13}$$

These equations consider linear intensity profiles inside each spatial mesh cell (an approximation which has increasing accuracy as the finite, delta r and z elements go to zero). Finally, once the intensities were obtained, the local volumetric rate of photon absorption (LVRPA, $e^{a,v}$) was calculated at each $r - z$ point of the reactor according to:

$$e^{a,v} = \int_{\lambda} \kappa_{\lambda}(\underline{x}) \cdot \int_{\Omega = 4\pi} I_{\lambda,\Omega}(\underline{x}) d\Omega d\lambda \quad \text{S14}$$